

# Nuclear fusion driven by Coulomb explosion of homonuclear and heteronuclear deuterium- and tritium-containing clusters

Isidore Last and Joshua Jortner

*School of Chemistry, Tel-Aviv University, Ramat Aviv, Tel Aviv 69978, Israel*

(Received 29 May 2001; published 6 November 2001)

The ionization and Coulomb explosion of homonuclear  $D_n$  and  $T_n$  ( $n=959-8007$ ) and heteronuclear  $(D_2O)_n$  and  $(T_2O)_n$  ( $n=459-2171$ ) clusters in very intense ( $I=5 \times 10^{14}-5 \times 10^{18} \text{ W cm}^{-2}$ ) laser fields is studied using classical dynamics simulations. The efficiency of the  $d+d$  and  $d+t$  nuclear fusion driven by the Coulomb explosion (NFDCE) is explored. The  $d+d$  NFDCE of  $(D_2O)_n$  heteronuclear clusters is enhanced by energetic and kinematic effects for  $D^+$ , while for  $(T_2O)_n$  heteronuclear clusters the kinetic energy of  $T^+$  is dominated by energetic effects. The cluster size dependence of the fusion reaction yield has been established. The heteronuclear clusters provide considerably higher  $d+d$  and  $d+t$  fusion reaction yields than the homonuclear clusters of the same size. The clusters consisting of both D and T atoms can provide highly efficient  $d+t$  fusion reactions.

DOI: 10.1103/PhysRevA.64.063201

PACS number(s): 36.40.Gk

## I. INTRODUCTION

Clusters irradiated by ultrashort (tens of fs) and ultraintense ( $I=10^{14}-10^{18} \text{ W cm}^{-2}$ ) laser pulses are subjected to multielectron ionization, which leads to Coulomb explosion of highly charged clusters [1-13]. The products of the Coulomb explosion are free electrons and high-energy atomic ions. The kinetic energy of the product ions is of the order of tens or hundreds eV in small clusters [1-4], and 10 keV-1 MeV in large clusters consisting of heavy atoms [5-11], reaching the energy domain of nuclear physics. In deuterium and tritium clusters, the products of the Coulomb explosion are high-energy deuterons and tritons, which may be capable of performing the fusion reactions [14]



The  $t+t$  reaction, whose cross section is very low [14], is not considered here. The  $d+d$  fusion reaction (1a) driven by the Coulomb explosion was proposed and detected by Zweiback *et al.*, who subjected large deuterium clusters (cluster radii  $R \sim 10-50 \text{ \AA}$ ) to an intense laser field ( $I \sim 5 \times 10^{17} \text{ W cm}^{-2}$ ) [12,13]. We proposed and demonstrated that an effective way to produce energetic deuterons for the  $d+d$  fusion reaction may involve the Coulomb explosion of molecular heteronuclear clusters of deuterium bound to heavy atoms, e.g.  $(D_2O)_n$  [15]. Similarly, the fusion reaction (1b) can be accomplished in mixed heteronuclear  $(D_2O)_n$  and  $(T_2O)_n$  or in  $(DTO)_n$  clusters. In all cases, the highly charged  $O^{6+}$  ions will provide a trigger for driving the  $D^+$  or  $T^+$  ions to high kinetic energies.

The nuclear fusion driven by Coulomb explosion (NFDCE) of deuterium or deuterium-tritium clusters can be realized by two different spatial configurations. In one configuration, the exploding cluster is located in the vicinity of a deuterium or a tritium target, so that the fusion reaction may take place when the  $d$  or  $t$  nuclei of these clusters penetrate

the target. Another configuration is made up of exploding clusters only. In this case, the collision of deuterons or tritons originating from different clusters may be responsible for the fusion reaction [12]. Such a configuration was used in the experiments of Zweiback *et al.* [12,13], where a considerably higher maximal  $dd$  (or  $tt$ ) collision energy, which is four times higher than the nuclei maximal energy in the laboratory frame, can be achieved.

The theoretical treatment of NFDCE address two distinct issues. First, one needs to know the energy spectrum of the light nuclei produced by the exploding clusters. Second, the fusion yield for a given energy spectrum of the nuclei has to be determined. When the cluster ionization is vertical, i.e., when the time scales for the cluster's outer ionization [16] and for the Coulomb explosion are separated [17-19], the energy spectrum can be grossly simplified and sometimes even expressed analytically. In this case, the explosion dynamics depends only on the interaction between the ions. In the case of nonvertical ionization, one also has to account for the electrons' dynamics. The simultaneous treatment of the motion of electrons and ions has been performed in the framework of the classical approach and applied to rare-gas clusters [16,20-22] and to deuterium-containing clusters [13,15]. The classical simulation of the ionization process and the cluster expansion provides the energy spectrum of the product ions. According to our findings [15], the energy spectrum of product deuterons is distinct from that of thermal motion, which questions the possibility of considering NFDCE as a thermonuclear process.

The energetics of the deuterons produced by the Coulomb explosion of  $D_n$  and of  $(D_2O)_n$  clusters was studied by us [15]. In this paper, we explore the NFDCE process, considering not only the energetics of the product ions but also the implications of the cluster ionization process on the dynamics of electrons and ions. We shall extend our previous studies [15] to consider high-energy dynamics of  $T^+$  ions from  $T_n$  homonuclear clusters and from  $(T_2O)_n$  heteronuclear clusters. The energetic spectrum of deuterons and tritons obtained by us is used for the determination of the yield for NFDCE.

## II. METHODOLOGY OF THE SIMULATIONS

The process of cluster ionization and Coulomb explosion involves three different kinds of particles: electrons bound to the host ions, unbound electrons, and ions. The unbound electrons and the ions are considered as classical particles [16,20,21]. The bound electrons, whose motion is of strictly quantum character, do not directly affect the process of cluster ionization and are of importance only as the source of the unbound electrons. The ionization of the bound electrons (i.e., the inner ionization process) is realized either by the suppression of the electrostatic barriers of the host ions [23] or by electron collision [22,24]. Since the tunneling has a minor effect on the ionization [25], the classical treatment of the dominating barrier suppression mechanism and collisional ionization becomes feasible. The classical approach allows us to describe both of the ionization mechanisms by simple models [16,20], where molecular-dynamics simulations of the unbound electrons are performed on the femtosecond time scale ( $10^{-15}$ – $10^{-12}$  sec), using attosecond and subattosecond ( $10^{-18}$ – $10^{-19}$  sec) time steps [16]. In molecular clusters, the barrier suppression mechanism for cluster multielectron ionization dominates over the collisional ionization mechanism [16,22]. The recombination process is expected to be of negligible importance [16,22] and can be ignored.

In the case of heavy atoms, a strong field removes not only valence-shell electrons but also some of the inner-shell electrons [2,6,7]. The simulation of the rare-gas  $Xe_n$  cluster ionization performed by us showed that in the intense fields of  $I \approx 10^{16} \text{ W cm}^{-2}$ , the outer-shell  $5s^2 5p^6$  electrons (ionization potentials  $IP \approx 12$ – $106 \text{ eV}$ ) are removed from the Xe atoms in several fs [16]. A much longer time scale, which is comparable with the time of the outer ionization (tens of fs), allows for the inner ionization of the  $d$  electrons ( $IP \geq 171 \text{ eV}$ ). To describe the multielectron laser-induced ionization of  $(D_2)_m$  [or  $(T_2)_n$ ] clusters, we shall consider the response of the “atomic”  $D_n$  (or  $T_n$ ),  $n = 2m$ , systems with the same atomic density. In the case of D atoms, inner ionization means the removal of one electron with an ionization potential of  $IP = 13.6 \text{ eV}$ . In our discussion, we will consider only D atoms, since the electronic properties of T atoms are the same. We found that the D atom is ionized when the field intensity is  $I \geq 1.5 \times 10^{14} \text{ W cm}^{-2}$ , which is close to the intensity required for the  $D_2$  molecule ionization [26]. In the fields of  $I \geq 5 \times 10^{14} \text{ W cm}^{-2}$  used in our simulations, the ionization of the D atom is realized in the very beginning of the first laser oscillation. In clusters where the ignition mechanism enhances inner ionization [27], the conditions for very fast ionization of the D atoms are even more favorable. The situation is different in the case of the  $(D_2O)_n$  clusters, where the time of inner ionization is determined by the ionization of O atoms. Since it is impossible to remove the inner  $O(1s)^2$  electrons ( $IP = 739$  and  $841 \text{ eV}$ ) in laser intensities of  $I \leq 5 \times 10^{15} \text{ W cm}^{-2}$  considered herein, we only take into account the ionization of outer shell  $O(2s)^2(2p)^4$  electrons, whose  $IP$ 's lie in the interval  $13.6$ – $138 \text{ eV}$ . One may expect that the ionization of these electrons occurs roughly on the same time scale as the ionization of the valence-shell elec-

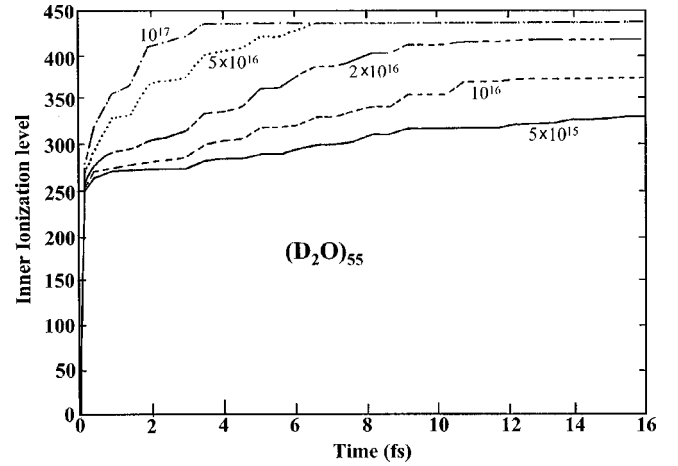


FIG. 1. Time evolution of inner ionization in the  $(D_2O)_{55}$  cluster for different laser intensities, as marked on the curves (in  $\text{W cm}^{-2}$ ). The inner ionization is described as the number of electrons  $N_e$  released from atoms. The complete ionization corresponds to  $N_e = 440$ .

trons of the Xe atoms in clusters [16], i.e., several fs.

In order to study the dynamics of the inner cluster ionization, we performed the simulation of this process in some of the  $D_n$  and  $(D_2O)_n$  clusters using the methodology of Ref. [16]. As expected, the ionization of the D atoms takes a very short time, e.g., 0.7 fs for the  $D_{959}$  cluster when subjected to an irradiation of  $I = 5 \times 10^{14} \text{ W cm}^{-2}$  at the pulse maximum. The dynamics of the inner ionization in the  $(D_2O)_{55}$  cluster is presented in Fig. 1 for  $5 \times 10^{15} < I < 10^{17} \text{ W cm}^{-2}$ . The cluster atoms lose most (about  $N_e \sim 250$ – $280$ ) of their 440 valence electrons in less than 0.3 fs (Fig. 1). This implies that in the very beginning of the pulse, every D atom loses its single electron and the O atoms lose the first two or three electrons. Subsequent ionization is slower and intensity dependent, reaching the saturation level at 4 and 16 fs for  $I = 10^{17}$  and for  $I = 5 \times 10^{15} \text{ W cm}^{-2}$ , respectively. At  $I \geq 5 \times 10^{16} \text{ W cm}^{-2}$  all D and O atoms are fully ionized [except for the inner  $O(1s)^2$  electrons, as was already mentioned]. At lower intensities, all six electrons are not removed from the O atoms, e.g., at  $I = 10^{16} \text{ W cm}^{-2}$  an average of 4.8 electrons are removed. When the inner ionization process removes all valence electrons from the D and O atoms, which occurs on a time scale of several fs, the approximation of the sudden inner cluster ionization (SICI) can be accepted.

The SICI approximation implies that at the starting point for the outer cluster ionization and the temporal onset of the Coulomb explosion ( $t = 0$ ), all relevant electrons are already removed from their host atoms. Such an approach significantly simplifies the simulation, excluding the initial stage of the inner ionization process [21]. We also assume that at the starting point the electrons, which are removed from the atoms, can be considered as unbound electrons located motionless in the proximity of their host atoms. In order to check the validity of the SICI approximation, we performed not only the simulation for some clusters in this approximation, but also the complete simulation, including the inner ionization process [16]. The results of these simulations are shown

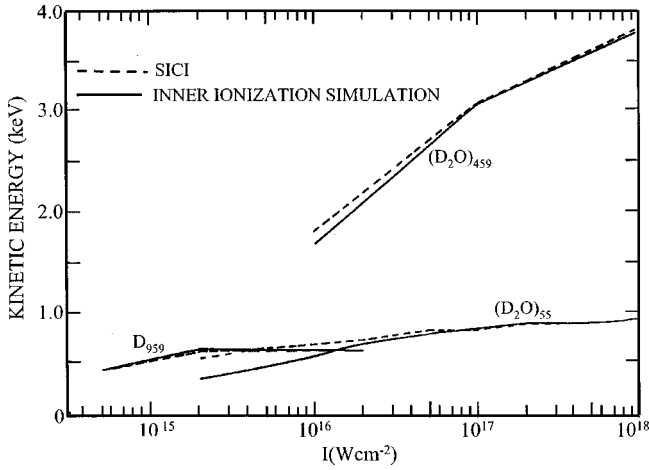


FIG. 2. The dependence of the maximal kinetic energy  $E_M$  of the product ions  $D^+$  on the laser intensity  $I$  for the clusters  $D_{959}$ ,  $(D_2O)_{55}$ , and  $(D_2O)_{459}$ . Solid lines, simulations with inner ionization (methodology of Ref. [20]); broken lines, simulations for the sudden inner cluster ionization (SICI).

in Fig. 2 where the maximal kinetic-energy  $E_M$  of the product  $d$  nuclei is presented. The differences between the  $E_M$  values obtained by the complete and by the SICI simulations are of no importance in the homonuclear  $D_{959}$  cluster. In the case of the heteronuclear  $(D_2O)_{55}$  and  $(D_2O)_{459}$  clusters, both simulations provide practically the same results at intense fields, however, the differences increase for lower laser intensities. As expected, the SICI approach overestimates the  $d$  (or  $t$ ) kinetic energies at lower laser intensities ( $I < 10^{17} \text{ W cm}^{-2}$ ). The accuracy of this approach is better for the relatively large  $(D_2O)_{459}$  cluster than for the small  $(D_2O)_{55}$  cluster. Our results support the application of the SICI approximation for homonuclear  $D_n$  clusters at  $I \geq 5 \times 10^{15} \text{ W cm}^{-2}$  and for heteronuclear  $(D_2O)_n$  clusters at  $I \geq 10^{16} \text{ W cm}^{-2}$ . Subsequent to inner cluster ionization (which can be handled by the SICI approximation for  $I \geq 10^{16} \text{ W cm}^{-2}$ ), outer cluster ionization occurs. At this stage, the approximation of vertical cluster ionization may be introduced, which involves the separation of the time scales between the removal of all unbound electrons produced by inner ionization and cluster expansion. This approximation will be discussed in Sec. III.

In highly multicharged clusters, the Coulomb potential becomes the dominant interaction [16,21], in contrast to the singly or doubly charged clusters [28,29]. The Coulomb potentials of the electron-electron and electron-ion interactions are slightly modified in order to avoid a steep increase in the forces at small distances, which may violate the energy conservation [16]. In the SICI approach, the final size of the ions (in our case,  $O^{6+}$  ions) is ignored.

Neglecting the molecular structure of the homonuclear  $A_n$  ( $A=D, T$ ) clusters, we assume that the atoms are uniformly distributed with the atomic density equal to that of liquid deuterium [30], which is  $\rho \approx 0.05 \text{ \AA}^{-3}$ . Here, we treat the following homonuclear  $D_n$  and  $T_n$  clusters (with the neutral cluster radius  $R_0$ ):  $n=959, R_0=16.6 \text{ \AA}$ ;  $n=1961, R_0=21.1 \text{ \AA}$ ;  $n=3367, R_0=25.4 \text{ \AA}$ ;  $n=8007, R_0=34 \text{ \AA}$ . The

$R_0$  values are somewhat lower than those originally used by us [15], which utilized the density of  $\rho=0.03 \text{ \AA}^{-3}$ . The heteronuclear  $(A_2O)_n$  ( $A=D, T$ ) clusters are described here as made up of uniformly distributed  $A_2O$  molecules with an AO distance of  $0.97 \text{ \AA}$  and an A-O-A angle of  $90^\circ$ . The density of the  $(A_2O)_n$  clusters is taken to be equal to the density of liquid water, e.g.,  $\rho \approx 0.035 \text{ \AA}^{-3}$  per molecule. We treat here the following heteronuclear  $(D_2O)_n$  and  $(T_2O)_n$  clusters (with the number  $N_e$  of valence electrons):  $n=459, R_0=14.8 \text{ \AA}, N_e=3672$ ;  $n=1061, R_0=19.8 \text{ \AA}, N_e=8488$ ;  $n=2171, R_0=25 \text{ \AA}, N_e=17368$ . The results are not expected to be sensitive to the simplifications for the structure of the clusters used here. In view of the Coulomb character of the long-range inter-particle forces, the interior interaction with the neighboring ions makes a minor contribution to the potential. For example, the  $D^+-D^+$  potential for the interatomic distance of the  $D_2$  molecule ( $r=0.74 \text{ \AA}$ ) is about  $19 \text{ eV}$ , whereas the kinetic energy of the product ions from the  $D_n$  clusters considered by us exceeds  $500 \text{ eV}$  [15]. Accordingly, the ion dynamics is insensitive to the short-range structural details.

Calculations were performed for a Gaussian-shaped laser pulse with a temporal half full width at a half maximum of  $25 \text{ fs}$  and intensities in the range  $I=5 \times 10^{14} - 5 \times 10^{18} \text{ W cm}^{-2}$ . The field frequency is  $\nu=0.35 \text{ fs}^{-1}$ . Taking into account that the radii of the clusters considered by us are much smaller than the penetration depth of the laser radiation [25], we consider the light intensity as being independent of the spatial coordinates.

### III. COULOMB EXPLOSION OF HOMONUCLEAR CLUSTERS

The description of the Coulomb explosion of homonuclear clusters is simple in the case of vertical ionization. For a homonuclear cluster of radius  $R_0$ , with identical charges  $q$  on each atom and a uniform atomic density  $\rho$ . The velocity is maximal for the ions at the cluster surface. The distance of these ions from the cluster center determines the cluster radius  $R(t)$ . When the ionization is vertical, the radius  $R(t)$  at time  $t$  is determined by the equations [12,19]

$$t = (A/q)(m/\rho)^{1/2} Z(\xi), \quad \xi = R_0/R(t), \quad (2)$$

$$Z(\xi) = \frac{(1-\xi)^{1/2}}{\xi} + \frac{1}{2} \ln \left( \frac{1+(1-\xi)^{1/2}}{1-(1-\xi)^{1/2}} \right). \quad (3)$$

We will use here the following units: the mass of a constituent (atom)  $m$  in  $AM$ , the constituent charge  $q$  in  $e$ , distance in  $\text{\AA}$  and consequently the density  $\rho$  in  $\text{\AA}^{-3}$ , and  $t$  in fs. The coefficient of Eq. (2) is then  $A=0.931 \text{ fs \AA}^{-3/2}$ . The time of the cluster radius doubling [ $\xi=0.5, Z(\xi)=2.296$ ] is

$$\tau = t(2R_0) = 2.137 q^{-1} (m/\rho)^{1/2}. \quad (4)$$

This time does not depend on the cluster radius and equals  $13.5$  and  $16.6 \text{ fs}$  for deuterium and tritium clusters, respectively. The time  $\tau$  defines the condition for vertical ionization

$$t_{oi} \ll \tau, \quad (5)$$

where  $t_{oi}$  is the time of the outer ionization of the cluster.

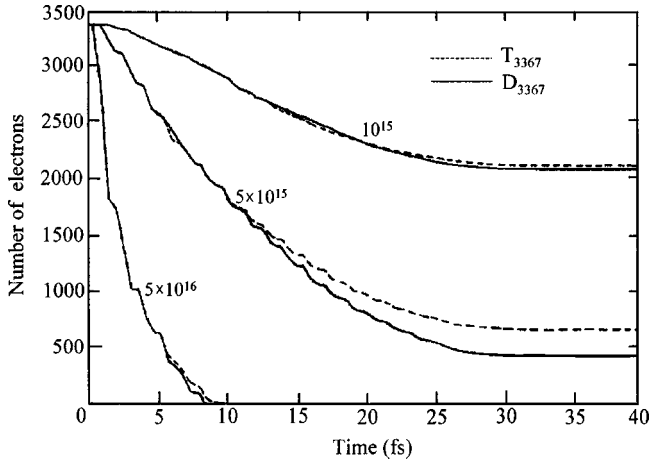


FIG. 3. The time evolution of the outer ionization in the  $D_{3367}$  and  $T_{3367}$  clusters for different laser intensities  $I$ , as marked on the curves (in  $\text{W cm}^{-2}$ ). The outer ionization process is described as the number of electrons bound to a cluster.

The dynamics of the outer ionization of the  $D_{3367}$  and  $T_{3367}$  clusters ( $R_0 = 25.4 \text{ \AA}$ ) is shown in Fig. 3. The outer ionization is recorded when the distance between an electron and the cluster center is six times larger than the cluster radius  $R(t)$ . At  $I = 5 \times 10^{16} \text{ W cm}^{-2}$  the time of the outer ionization is  $t_{oi} \approx 8 \text{ fs}$ , meeting the validity condition for vertical ionization, Eq. (5). At  $I = 5 \times 10^{15} \text{ W cm}^{-2}$ , the clusters lose almost all electrons. However, the ionization time  $t_{oi}$  is comparable to the expansion time  $\tau$  violating the vertical ionization condition of Eq. (5). At  $I = 10^{15} \text{ W cm}^{-2}$ , the ionization is far from being vertical, which is not only due to the violation of Eq. (5) but also because the clusters lose only about 40% of their electrons.

The dynamics of outer ionization (Fig. 3) affects the dynamics of the cluster Coulomb explosion. The cluster expansion, which is quantified by  $R(t)$ , is shown in Fig. 4 together with  $R(t)$  for vertical ionization, given by Eq. (2). According to the results presented in Fig. 4, the Coulomb explosion dynamics of  $D_{3367}$  and  $T_{3367}$  clusters is close to the vertical ionization dynamics for  $I = 5 \times 10^{16} \text{ W cm}^{-2}$ , but is far from it at the relatively low intensity of  $I = 10^{15} \text{ W cm}^{-2}$ . For the Coulomb explosion following vertical ionization, the D/T isotope effect inferred from Eq. (4) is  $\tau \propto m^{1/2}$ . The isotope effect is clearly evident by comparing Figs. 4(a) (deuterium) and 4(b) (tritium). The dependence of the doubling radius time  $\tau$  on the laser intensity  $I$  for  $D_{3367}$  and  $T_{3367}$  clusters is shown in Fig. 5. The isotope effect  $\tau_T/\tau_D = (m_T/m_D)^{1/2} = 1.225$  is almost exactly fulfilled, with a very slight decrease when the laser intensity  $I$  decreases.

For the outer ionization dynamics (Fig. 3), the isotope effect is weakly exhibited. Such behavior can be rationalized by asserting that the most effective ionization process takes place when the cluster radius  $R(t)$  is not much larger than the initial  $R_0$  value and, consequently, is almost the same for different isotopes. This means that in the  $D_n$  and  $T_n$  clusters, the expansion does not enhance the outer ionization, in contrast to our previous findings for the  $\text{Xe}_n$  clusters [16].

The dependence of the ionization dynamics on the laser

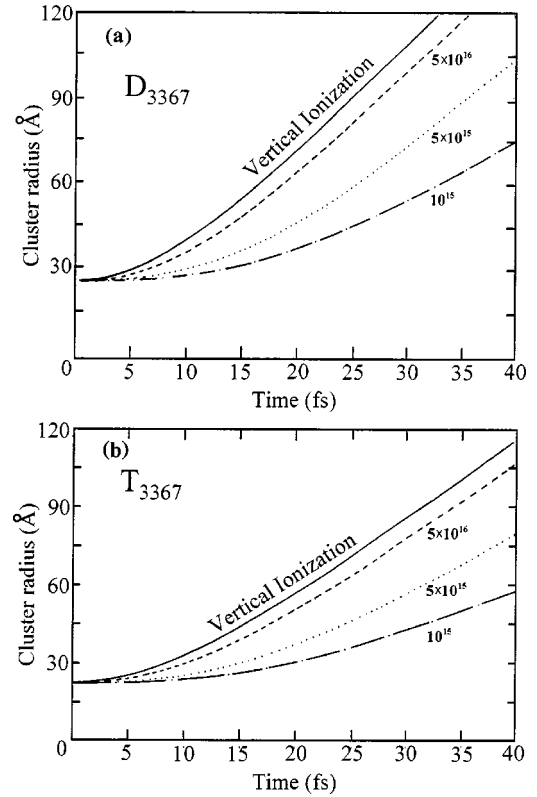


FIG. 4. Time evolution of cluster radius for different laser intensities  $I$ , as marked on the curves (in  $\text{W cm}^{-2}$ ). (a) Deuterium  $D_{3367}$  cluster. (b) Tritium  $T_{3367}$  cluster.

intensity discussed above has to be manifested in some way also in the energetics of the unbound electrons. Initially, at  $t=0$ , the unbound electrons are at rest forming a neutral zero-temperature plasma with the cluster. Due to the energy pumping from the laser irradiation, the kinetic energy of these electrons increases in time and some of them begin to leave the cluster. Some examples for the average kinetic-energy  $\bar{E}_e(t)$  evolution of the unbound electrons located inside the cluster are presented in Fig. 6. The most striking

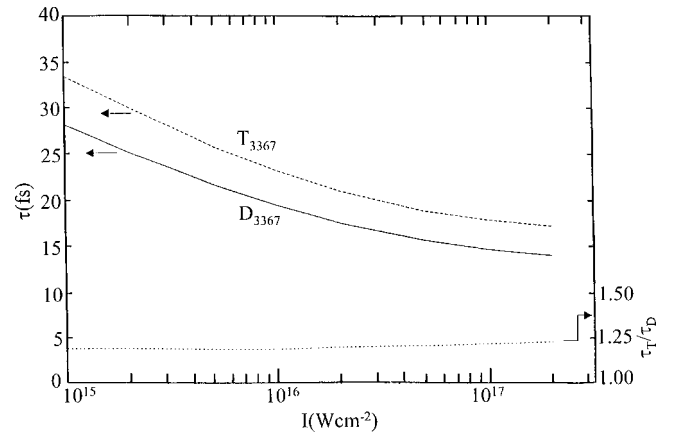


FIG. 5. The dependence of the time  $\tau$  of cluster radius doubling for the  $D_{3367}$  and  $T_{3367}$  clusters (left scale) and of the tritium/deuterium times  $\tau$  relation  $\tau_T/\tau_D$  (right scale) on the laser intensity  $I$ .

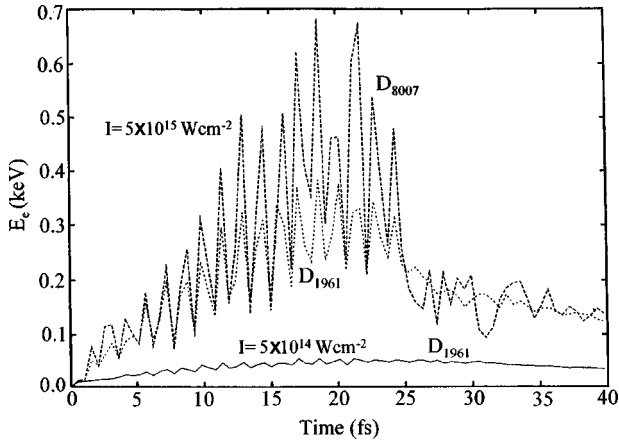


FIG. 6. The time evolution of the average kinetic energy  $\bar{E}_e$  of electrons located inside a cluster for  $D_{1961}$  and  $D_{8007}$  clusters subjected to different laser intensities  $I$ .

feature of the  $\bar{E}_e(t)$  evolution is the oscillations, whose amplitude increases with laser power  $I$ . In the time interval of the pulse action ( $0 \leq t \leq 25$  fs) these oscillations are clearly generated by the laser field. In the absence of radiation ( $t > 25$  fs), strong oscillations are exhibited for the strong intensity of  $I = 5 \times 10^{15} \text{ W cm}^{-2}$ . In the case of a relatively weak intensity of  $I = 5 \times 10^{14} \text{ W cm}^{-2}$ ,  $\bar{E}_e(t)$  demonstrates small oscillations in the presence of the pulse and changes smoothly after the pulse ceases ( $t > 25$  fs).

Examples for the energy distribution  $P_e(E)$  of the unbound electrons inside a cluster are displayed in Fig. 7 together with the thermal distribution  $P_{\text{th}}(E)$  for the same average energy  $\bar{E}_e$ ,

$$P_{\text{th}}(E) = 2\pi^{-1/2}(\bar{E}_e)^{-3/2}E^{1/2}\exp[-E/\bar{E}_e]. \quad (6)$$

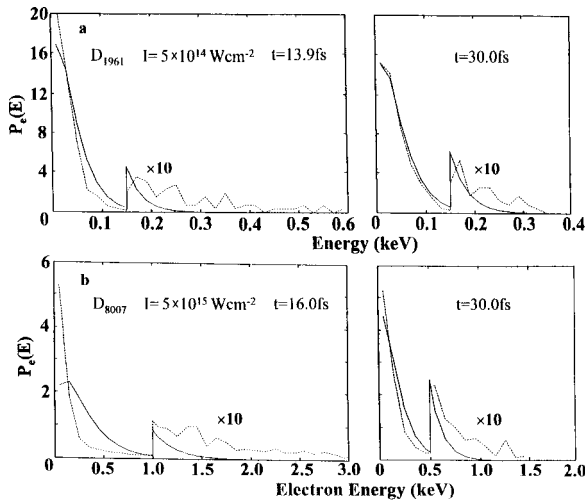


FIG. 7. The kinetic-energy distribution  $P_e(E)$  of electrons located inside a cluster. Broken lines represent the simulation results, solid lines represent the thermal distribution for the average kinetic energy  $\bar{E}_e$  of the simulation results.  $P_e(E)$  are normalized to unity. (a)  $D_{8007}$ ,  $I = 5 \times 10^{15} \text{ W cm}^{-2}$ ;  $t = 16$  fs ( $\bar{E}_e = 0.300$  keV) and  $t = 30$  fs ( $\bar{E}_e = 0.164$  keV). (b)  $D_{1961}$ ,  $I = 5 \times 10^{14} \text{ W cm}^{-2}$ ;  $t = 13.9$  fs ( $\bar{E}_e = 0.042$  keV) and  $t = 30$  fs ( $\bar{E}_e = 0.047$  keV).

In the intense fields of  $I = 5 \times 10^{15}$  [Fig. 7(b)], energy distribution of the electrons differs significantly from the thermal distribution, first of all, during the pulse action ( $t = 16$  fs). The maximal value of  $P_e(E)$  is reached at  $E = 0$ , with a steep drop at  $E < 0.4$  keV. At  $E > 0.4$  keV  $P_e(E)$  begins to decrease slowly becoming by orders of magnitude larger than the thermal distribution at the high energy “tail.” Although the electrons of the high-energy “tail” make up only for a small fraction of the total number of electrons, they are of prime importance for the process of outer ionization. The situation is different in the case of laser intensity  $5 \times 10^{14} \text{ W cm}^{-2}$ , where the energy distribution  $P_e(E)$  becomes more similar to the thermal distribution. However, even at this low intensity, the number of high-energy electrons is considerably larger than for the thermal distribution. The  $P_e(E)$  patterns are most probably affected by Coulomb fields of positively charged cluster. These fields tend to slow down the radial motion of electrons passing the cluster periphery and to speed up electrons passing the cluster center. The results presented in Figs. 6 and 7 allow us to conclude that the application of the thermal plasma theory to the cluster ionization [4,8,25] is not well founded.

The ability of the product  $d$  or  $t$  nuclei to contribute to the fusion is determined by their kinetic energy. In the case of vertical ionization, the final kinetic energy of an ion ( $D^+$  or  $T^+$ ) is equal, with the opposite sign, to its initial potential energy. Under the conditions of the Coulomb explosion following cluster vertical ionization, the kinetic energy (per ion in eV) of ions at the initial distance  $R$  is given by [13,15,19,20]

$$E(R) = (4\pi/3)Bq^2\rho R^2, \quad (7)$$

where  $B = 14.385 \text{ eV \AA}$ . The energy  $E_M$  is maximal for ions initially located at the cluster surface (at  $R = R_0$ ), being given by

$$E_M = (4\pi/3)Bq^2\rho R_0^2. \quad (7a)$$

Equation (7a) provides a unique case of a cluster size equation (CSE) [31,32], with the scaling law  $E_M \propto R_0^2$  constituting an exception for CSEs, which usually converge to the condensed phase ( $R_0 \rightarrow \infty$ ) limit. We expected that  $E_M \propto R_0^2$  is inferred on the basis of simple electrostatic arguments and  $E_M$  does not exhibit a D/T isotope effect. As we have already demonstrated, the conditions for the vertical ionization are realized at strong laser intensities. At lower intensities, when the ionization is not vertical, the maximal kinetic-energy  $E_M$  is lower than that given by Eq. (7a). This feature of the Coulomb explosion is well demonstrated in Fig. 8(a), which presents the maximal kinetic-energy  $E_M$  dependence on the laser intensity  $I$ . Figure 8(a) reveals an increase of  $E_M$  with increasing  $I$  at lower  $I$  followed by saturation at high  $I$ . The saturation values  $E_M$  almost coincide with the  $E_M$  of Eq. (7a). The  $I$  interval, where  $E_M$  begins to decrease markedly with decreasing  $I$ , is cluster-size dependent and determines the upper limit for an efficient Coulomb explosion. The  $I$  value, which determines these limits quantitatively, was chosen as the intensity  $I_e$ , where the kinetic-energy  $E$  makes up

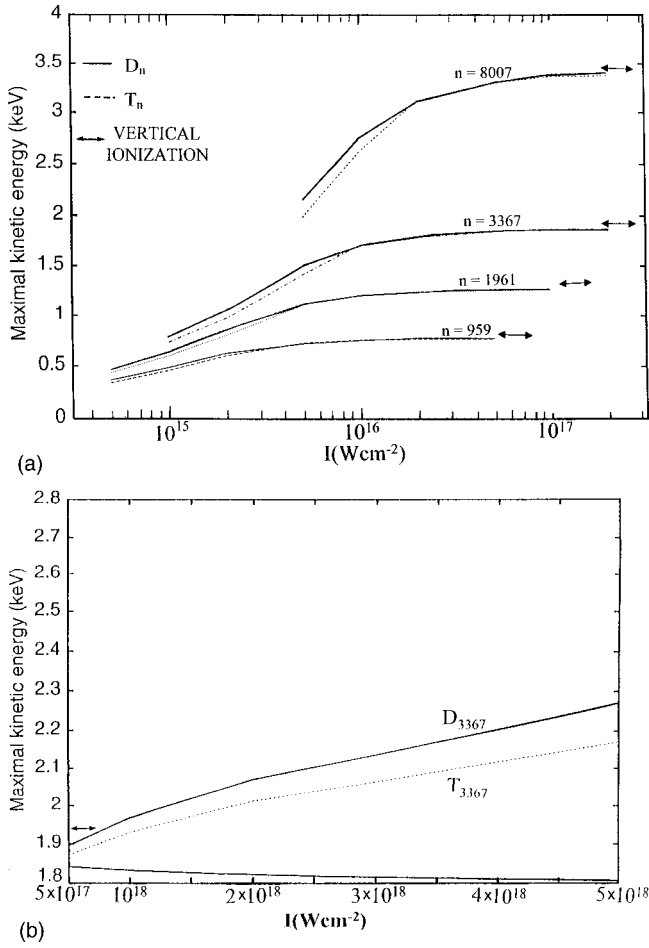


FIG. 8. The dependence of the maximal kinetic-energy  $E_M$  of  $D^+$  and  $T^+$  ions on the laser intensity  $I$  for homonuclear clusters  $D_n$  and  $T_n$ , respectively. The vertical ionization values  $E_M$  of Eq. (7a) are marked by horizontal arrows. (a) Laser intensity interval  $I=5 \times 10^{14} \text{ W cm}^{-2} - 2 \times 10^{17} \text{ W cm}^{-2}$ ,  $n=959, 1061, 3367, 8007$ . (b) Laser intensity interval  $I=5 \times 10^{17} \text{ W cm}^{-2} - 5 \times 10^{18} \text{ W cm}^{-2}$ ,  $n=3367$ . The bottom curve shows  $E_M$  when the ions are not subjected to a laser field.

for 85% of the saturation level [15]. The intensity  $I_e$  follows the quadratic-size dependence, such as  $E_M$  in Eq. (7a) [15]. In the regions of  $I \sim I_e$  and  $I < I_e$ , the kinetic energies are a little lower for the tritium clusters than for the deuterium clusters [Fig. 8(a)], while for  $I > I_e$ , no isotope effect on the  $E_M$  vs  $I$  dependence is exhibited.

The saturation behavior of the  $E_M$  energy dependence on laser intensity  $I$  is demonstrated in Fig. 8(a) for  $I \leq 2 \times 10^{17} \text{ W cm}^{-2}$ . This saturation behavior is, however, violated at very strong intensities,  $I \geq 5 \times 10^{17} \text{ W cm}^{-2}$ , as shown in Fig. 8(b) for  $D_{3367}$  and  $T_{3367}$  clusters, where  $E_M$  further increases by about 15% in the intensity range  $I=5 \times 10^{17} \text{ W cm}^{-2} - 5 \times 10^{18} \text{ W cm}^{-2}$ . This increase is roughly proportional to  $I$  and it reveals a distinct isotope effect. In order to check the cause of this increase of  $E_M$ , we present in Fig. 8(b) also the results of a calculation, where ions are not exposed to the laser field. In this latter case,  $E_M$  does not increase with  $I$ . It follows that at  $I \geq 5 \times 10^{17} \text{ W cm}^{-2}$ , the electrons' pressure on the ions (hydrodynamic effect) is of no

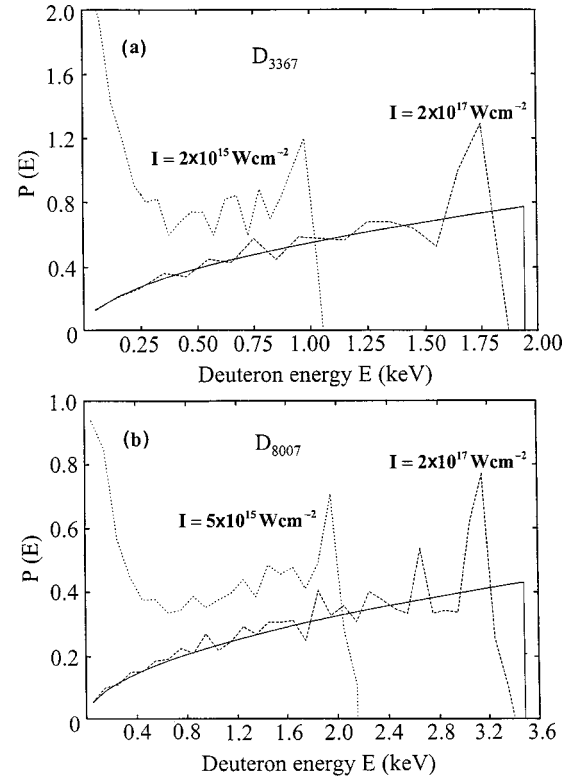


FIG. 9. The kinetic-energy distribution  $P(E)$  of  $D^+$  ions for homonuclear  $D_n$  clusters. Broken lines present the simulation results; the solid line presents the vertical ionization distribution of Eq. (8).  $P(E)$  are normalized to unity. (a)  $D_{3367}$  cluster, laser intensities  $I=2 \times 10^{15}$  and  $2 \times 10^{17} \text{ W cm}^{-2}$ . (b)  $D_{8007}$  cluster, laser intensities  $I=5 \times 10^{15}$  and  $2 \times 10^{17} \text{ W cm}^{-2}$ .

importance and that the direct effect of the laser field on the ions is responsible for the  $E_M$  increase.

Using Eqs. (7) and (7a) it is possible to determine the energy spectrum of the product nuclei for the case of vertical ionization

$$P(E) = \frac{3}{2} (E/E_M^3)^{1/2}, \quad E \leq E_M, \quad (8)$$

$$P(E) = 0, \quad E > E_M. \quad (8a)$$

The distribution  $P(E)$  of Eq. (8) is normalized to unity. According to this equation,  $P(E)$  increases with  $E$  as  $E^{1/2}$  at  $E < E_M$ . The average energy of the distribution (8) is  $\bar{E} = (3/5)E_M$ . The energy spectra of ions produced by the Coulomb explosion are shown in Fig. 9 for the  $D_{3367}$  [Fig. 9(a)] and  $D_{8007}$  [Fig. 9(b)] clusters for different laser intensities, together with the  $P(E)$  distributions of Eq. (8). We expect that the  $P(E)$  distributions at very intense fields of  $I=2 \times 10^{17}$  are close to those given by Eq. (8). At lower intensities, ( $I=2 \times 10^{15}$  and  $5 \times 10^{15} \text{ W cm}^{-2}$  for  $n=3367, 8007$ , respectively), when the ionization is far from being vertical (Fig. 8) and the maximal energy is sufficiently lower than that of Eq. (7a), the curve's shape does not follow the  $E^{1/2}$  dependence of Eq. (8), demonstrating a strong increase of  $P(E)$  for  $E \rightarrow 0$ . Such  $P(E)$  behavior can be explained by incomplete ionization (Fig. 3) resulting in screening effects by the electrons remaining inside the cluster. These contrib-

ute to the formation of an almost neutral body, most probably in the cluster center, preventing the acceleration of the ions located there. According to our simulations, the energy spectra of the ions generated by the Coulomb explosion is drastically different from the thermal energy spectrum, mainly with respect to the high-energy “tail,” which is of the prime importance for thermonuclear fusion [14,33]. This feature of the Coulomb explosion is expected to affect significantly the NFDCE process, as discussed in Sec. VI.

#### IV. COULOMB EXPLOSION OF HETERONUCLEAR CLUSTERS

Equation (7) implies that the ion kinetic energy increases strongly with the ionic charge  $q$ , i.e.,  $E_M \propto q^2$  [13,15,19,22] for homonuclear equally charged clusters. Accordingly, multielectron atoms, which can be highly ionized, provide ions of considerably higher kinetic energy than the one-electron atoms. For example, the maximal energy of the  $\text{Xe}^{q+}$  ions produced by the  $\text{Xe}_{1061}$  cluster is  $\sim 40$  keV (for  $q=17$ ) [16], whereas in the case of  $\text{D}^+$  ions from the similar size  $\text{D}_{959}$  cluster, this energy is only 0.77 keV (Fig. 8). In order to produce energetic ions of one-electron atoms, we recently proposed to use the heteronuclear molecular clusters  $(A_l B_k)_n$  consisting of  $A_l B_k$  molecules with light one-electron  $A$  ( $A = \text{D}$  or  $\text{T}$ ) atoms and heavy multielectron  $B$  atoms [15]. The enhancement of the energy of  $\text{D}^+$  or  $\text{T}^+$  ions from the Coulomb explosion of multicharged  $(A_l B_k)_n$ ,  $A = \text{D}, \text{T}$  heteronuclear clusters can originate from kinetic-energy enhancement and from kinematic effects [15]. Consider first the kinetic-energy enhancement. The multicharged  $\text{B}^{-q_B}$  ions drive the light  $\text{A}^+$  ions to high kinetic energies. In this study, we will consider the electronic and nuclear dynamics of the heteronuclear heavy water clusters  $(A_2 \text{O})_n$ ,  $A = \text{D}, \text{T}$ . Considering only the energetic effect then, in analogy with the homonuclear clusters, Eq. (7a), the light  $\text{A}^+ = \text{D}^+$  ions on the cluster surface will gain the maximal energy of

$$E(R_0) = (4\pi/3)B(2q_A + q_O)\rho_O q_A R_0^2, \quad (9)$$

with  $q_A = 1$ ,  $q_O = 6$ , and  $\rho_O$  being the molecular (or O-atom) density. Thus, the energetic enhancement for the Coulomb explosion for heteronuclear clusters relative to homonuclear clusters of the same radius is  $(2q_A + q_O)\rho_O/q_A \rho_A = 5.6$ . Next, we focus on kinematic effects. The acceleration of light (mass  $m_A$ ) and of heavy (mass  $m_B$ ) ions located at the same distance from the cluster center is related by the kinematic parameter

$$\eta = q_A m_B / q_B m_A. \quad (10)$$

The light ions attain a higher velocity than the heavy ions for  $\eta > 1$ . When the atoms are deprived from all valence electrons, this condition is met in the deuterium case ( $A = \text{D}$ ,  $m_A = 2$ ) for all heavy  $B$  atoms in the periodic table, beginning from Li. In the case of tritium atoms ( $A = \text{T}$ ,  $m_A = 3$ ) the condition  $\eta > 1$  is not fulfilled for the following five heavy atoms (the corresponding  $\eta$  values are given in parentheses):  $^{12}\text{C}$  (1.0),  $^{14}\text{N}$  (0.93),  $^{16}\text{O}$  (0.89),  $^{19}\text{F}$  (0.90), and  $^{23}\text{Ne}$  (0.96). The difference in the  $\eta$  parameters of the

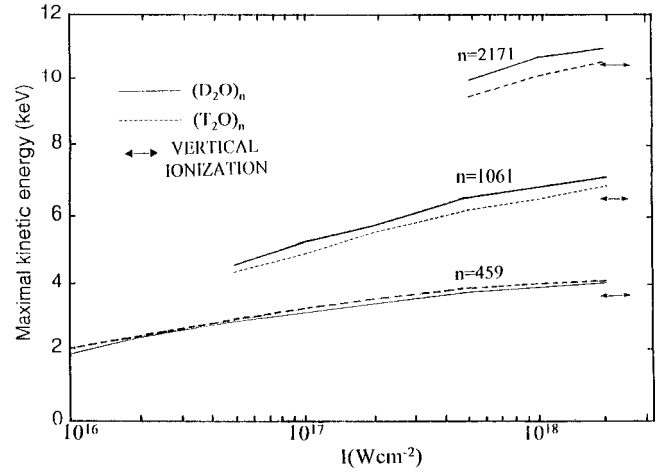


FIG. 10. The dependence of the  $\text{D}^+$  and  $\text{T}^+$  maximal kinetic energy  $E_M$  on the laser intensity  $I$  for heteronuclear  $(\text{D}_2\text{O})_n$  and  $(\text{T}_2\text{O})_n$  clusters, respectively. The  $E_M$  values of Eq. (10) are marked by horizontal arrows.

deuterium- and tritium-containing clusters affects the character of their Coulomb explosion.

In the case of the  $(\text{D}_2\text{O})_n$  clusters ( $\eta = 1.33$ ), a substantial portion of the  $\text{D}^+$  ions are expected to move out from the initial configurational framework of the  $\text{O}^{6+}$  ions, forming the outer shell of the expanding cluster. Provided that the cross section for  $\text{D}^+ + \text{O}^{6+}$  collisions is sufficiently small [34], some of the  $\text{D}^+$  ions initially located inside the cluster ( $R < R_0$ ) may overrun not only the heavy ions but also the  $\text{D}^+$  ions located initially further from the center. The kinematic effect results in the further enhancement of the maximal kinetic energy of  $\text{D}^+$  ions from heteronuclear clusters. The inner  $\text{D}^+$  ions, which overrun the periphery ions, gain higher energy than the latter ones, so that the maximal kinetic energy of the product  $\text{D}^+$  ions may exceed the energy given by Eq. (9).

The dependence of the maximal kinetic energy  $E_M$  of the product  $\text{D}^+$  ions on the laser intensity  $I$  is presented in Fig. 10. The heteronuclear clusters provide a significantly higher  $E_M$  energy than the homonuclear clusters of roughly the same size. For example, the  $\text{D}_{3367}$  and  $(\text{D}_2\text{O})_{2171}$  clusters, both of  $R_0 \sim 25 \text{ \AA}$ , provide deuterons with  $E_M \approx 1.8$  and  $E_M \approx 11$  keV, respectively. The  $E_M$  energy approximately obeys the CSE relation  $E_M \propto R_0^2$  dependence for a given intensity  $I$  [15]. The  $E_M(I)$  dependence on  $I$  does not exhibit saturation so that the  $E_M(I)$  energy curves cross the level of Eq. (9), marked in Fig. 10. Such behavior is due to the direct effect of the laser field on the ions [see Fig. 8(b)]. Some contribution to the  $E_M$  increase with  $I$  may provide kinematic effects, i.e., the ability of the inner ions to overrun the periphery ions, as discussed above. This kinematic feature of heteronuclear clusters affects also the energy spectrum  $P(E)$  of product ions.

The energy spectrum of  $(\text{D}_2\text{O})_n$  clusters [Fig. 11(a)] exhibits a large maximum located close to the maximal energy  $E_M$ . Consequently, the energy of most of the product deuterons lies in a relatively narrow high-energy interval. Such an energy distribution is in marked contrast with the broad

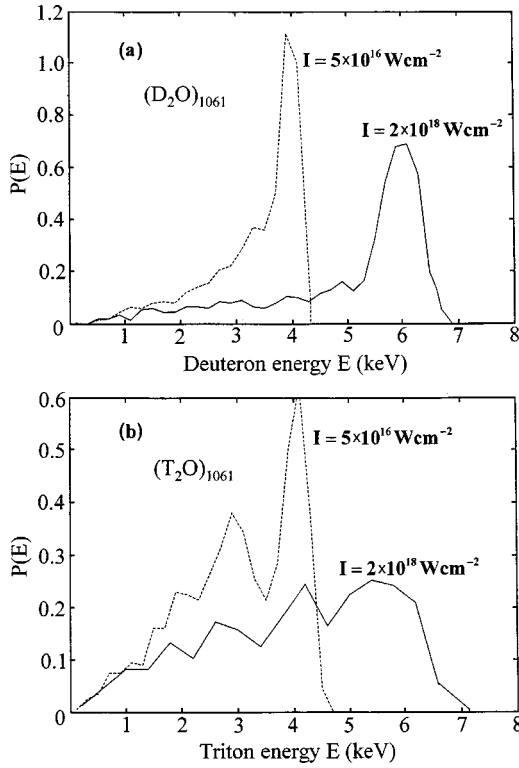


FIG. 11. The kinetic-energy distribution  $P(E)$  of  $D^+$  and  $T^+$  ions for heteronuclear clusters. Laser intensities  $I = 5 \times 10^{16}$  and  $2 \times 10^{18} \text{ W cm}^{-2}$ .  $P(E)$  are normalized to unity. (a)  $D^+$  ions for  $(D_2O)_{1061}$  cluster. (b)  $T^+$  ions for  $(T_2O)_{1061}$  cluster.

$P(E)$  curves of the homonuclear  $D_n$  clusters (Fig. 9). The high-energy fraction of the energy spectrum will be described by a Gaussian,

$$P(E) = \frac{\gamma}{\theta E_M \sqrt{\pi}} \exp\left[-\left(\frac{E - \varepsilon E_M}{\theta E_M}\right)^2\right], \quad (11)$$

where  $\gamma$  stands for the fraction of ions whose energy lies inside the Gaussian. The parameters of Eq. (11) were estimated to be  $\gamma = 2/3$ ,  $\varepsilon = 0.85$ , and  $\theta = 0.08$ .

The Coulomb explosion in the  $(T_2O)_r$  clusters is expected to proceed by a different way than in the  $(D_2O)_n$  clusters because of the parameter  $\eta < 1$ , which prohibits the overrunning kinematic effect. In the  $(T_2O)_n$  cluster, the heavy  $O^{6+}$  ions are moving faster than the light  $T^+$  ions, whereas in the  $(D_2O)_n$  cluster, the opposite situation is realized. In spite of such differences in the ions' motion, the maximal energies  $E_M$  of the  $T^+$  ions are close to the  $E_M$  values of the  $D^+$  ions (Fig. 10). However, the energy spectra produced by the  $(T_2O)_n$  and  $(D_2O)_n$  clusters differ significantly (Fig. 11). The  $T^+$  energy distribution  $P(E)$  manifests a wide maximum [Fig. 11(b)]. Such an energy spectrum reduces the efficiency of the  $(T_2O)_n$  clusters as a source of energetic tritons for NFDCE.

## V. NUCLEAR FUSION RATES

In the NFDCE experiments, the fusion reaction is due to the collisions of energetic light nuclei ( $d$  or  $t$ ) produced from

different clusters [12,13,15]. The reaction starts when, due to the Coulomb explosion, the cluster diameters become comparable to the distance between clusters (time  $t_1$ ), and stops at some time  $t_2$ , when the nuclei begin to leave the reaction volume. In the time interval  $t_1 < t < t_2$ , the reaction volume can be described as a homogeneous gas of uniformly distributed nuclei and with randomly oriented velocities. The fusion rate in the homogeneous gas is

$$R = 1/2 \rho_r \langle \sigma v \rangle, \quad (12)$$

where  $v$  is the relative velocity of the colliding nuclei,  $\sigma$  is the fusion cross section, the angular brackets mean the average over the energy distribution of the colliding nuclei, and  $\rho_r$  is the atomic density inside the reaction volume  $V_r$  [35]. Ignoring the increase of the reaction volume  $V_r$ , we assume  $\rho_r$  to be constant and equal to  $\rho_r = N_r/V_r$ , where  $N_r$  is the total number of nuclei inside  $V_r$ . In the case of a gas consisting of both  $d$  and  $t$  nuclei the  $d+t$  (Eq. (1b)) fusion reaction rate is

$$R = p_t(1 - p_t) \rho_r \langle \sigma v \rangle, \quad (12a)$$

where  $p_t$  is the  $t$  nuclei fraction.

Averaging over the colliding particle energies  $E_1$  and  $E_2$  in the laboratory frame, and the collision angle  $\alpha$ , one obtains

$$\langle \sigma v \rangle = \frac{1}{2} \int_0^\infty P(E_1) dE_1 \int_0^\infty P(E_2) dE_2 \int_0^\pi \sigma(E) \times (2E/m)^{1/2} \sin(\alpha) d\alpha. \quad (13)$$

The collision energy  $E$ , which is required for the calculation of the fusion cross section, is

$$E = E_1 + E_2 - 2(E_1 E_2)^{1/2} \cos(\alpha). \quad (14)$$

In the case of the  $d+d$  fusion reaction (1a) the cross section  $\sigma(E)$  can be fitted analytically by the equation [36]

$$\sigma(E) = (S/E) \exp(-A/E^{1/2}). \quad (15)$$

Fitting the experimental  $\sigma(E)$  values for the  $d+d$  (1a) reaction [37,38] in the interval  $2 < E < 250 \text{ keV}$ , we found  $A = 45 \text{ keV}^{1/2}$  and  $S = 1.8 \times 10^{-22} \text{ cm}^2 \text{ keV}$ . Equation (15) was used by us to describe also the cross section of the  $d+t$  fusion reaction (1b). For this reaction in the interval  $1.6 < E < 130 \text{ keV}$ , we found the parameters  $A = 44 \text{ keV}^{1/2}$  and  $S = 3.4 \times 10^{-20} \text{ cm}^2 \text{ keV}$ .

Neglecting the effect of the nucleus-nucleus and nucleus-electron collisions on the nuclear motion and assuming the gas to be neutral, we also assume that the energy spectra  $P(E_1)$  and  $P(E_2)$  are identical to the energy spectrum of the product ions of individual clusters. In the case of homonuclear clusters, the energy spectrum  $P(E)$  is described by Eq. (8). Substituting Eqs. (8) and (15) into Eq. (13) and replacing  $E$  by  $X = E/E_M$  one obtains

$$\langle \sigma v \rangle = (S/E_M) S/E_M v_M G(T_M), \quad (16)$$

where

$$v_M = (2E_M/m)^{1/2}, \quad (17)$$

$$T_M = A/E_M^{1/2}, \quad (18)$$

$$G(T_M) = (9/8) \int_0^1 X_1^{1/2} dX_1 \int_0^1 X_2^{1/2} dX_2 \int_0^\pi X^{-1/2} \times \exp(-T_M/X^{1/2}) \sin(\alpha) d\alpha, \quad (19)$$

and

$$X = X_1 + X_2 - 2(X_1 X_2)^{1/2} \cos(\alpha). \quad (19a)$$

The reaction yield is

$$Y = RN\bar{Z}/\bar{v}, \quad (20)$$

where  $R$  is the reaction rate, Eq. (12),  $N$  is the number of nuclei in the reaction volume  $V_r$ ,  $\bar{Z}$  is the mean path of nuclei inside the reaction volume, and  $\bar{v}$  is the average velocity of the reaction active nuclei. In the NFDCE experiments [12,13], the atomic density is  $\rho = 2 \times 10^{19} \text{ cm}^{-3}$  and the reaction volume has the shape of a cylinder with height  $h = 0.2 \text{ cm}$  and radius  $r = 0.01 \text{ cm}$ , which provides the number of nuclei  $N = 1.2 \times 10^{15}$ . We estimated the mean path of a thin cylinder ( $r \ll h$ ) as  $\bar{Z} = 1/2\pi r$  (in Ref. [13],  $\bar{Z} = 2r$ ). The velocity  $\bar{v}$  is identified with the maximal velocity  $v_M$  of Eq. (17). For  $\bar{v}$  corresponding to the energy  $E_M = 10 \text{ keV}$ , for example, the time of existence of the reaction volume  $t_2 = \bar{Z}/\bar{v}$  is about 100 ps. According to our estimates the time of the onset of reaction, is considerably smaller, being about  $t_1 \approx 70 \text{ fs}$ .

In the case of heteronuclear  $(D_2O)_n$  clusters, the energy spectrum is described by a Gaussian function, Eq. (11). Substituting Eq. (11) into Eq. (13), we obtain the following expression for the function  $G(T_M)$ :

$$G(T_M) = \frac{\gamma^2}{2\pi\theta^2} \int_{2\varepsilon-1}^1 \exp\left[-\left(\frac{X_1-\varepsilon}{\theta}\right)^2\right] dX_1 \int_{2\varepsilon-1}^1 \times \exp\left[-\left(\frac{X_2-\varepsilon}{\theta}\right)^2\right] dX_2 \int_0^\pi X^{-1/2} \times \exp(-T_M/X^{1/2}) \sin(\alpha) d\alpha. \quad (21)$$

For heteronuclear clusters, we take the reaction volume parameters to be the same as in the case of homonuclear clusters.

The fusion reaction parameters were calculated not only for the  $d+d$  reaction but also for the much more efficient  $d+t$  reaction. In the case of the  $d+t$  reaction, we take an equal amount of  $d$  and  $t$  nuclei [ $p_t = 0.5$  in Eq. (12a)]. The  $\langle\sigma v\rangle$  and  $Y$  dependences on  $E_M$  are shown in Fig. 12 for homonuclear clusters only. The  $\langle\sigma v\rangle$  and  $Y$  dependences on  $E_M$  for heteronuclear clusters were found to be almost identical to those for homonuclear clusters, which indicates that the differences in the energy spectra (Figs. 9 and 11) are not of considerable importance for the yield of the fusion reac-

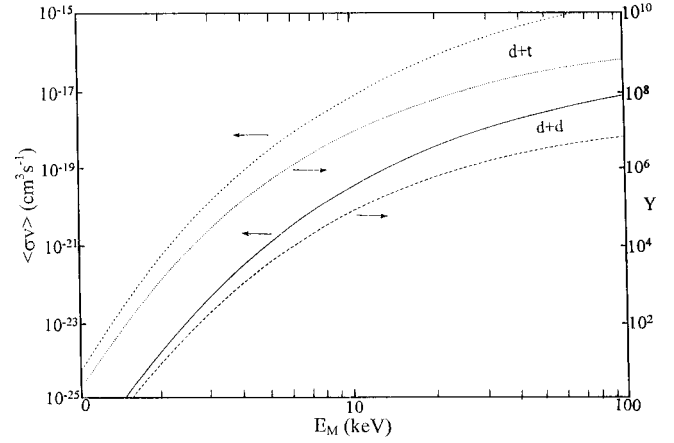


FIG. 12. The dependence of the nuclear fusion parameter  $\langle\sigma v\rangle$  (left scale) and the neutron yield  $Y$  (right scale) on maximal kinetic energy  $E_M$  of nuclei.

tion. The dependence of  $\langle\sigma v\rangle$  and  $Y$  on the cluster radius  $R_0$  is shown in Fig. 13. In the case of homonuclear clusters, the connection between  $R_0$  and  $E_M$  is determined for the conditions of vertical ionization [Eq. (7a)] whereas in the case of

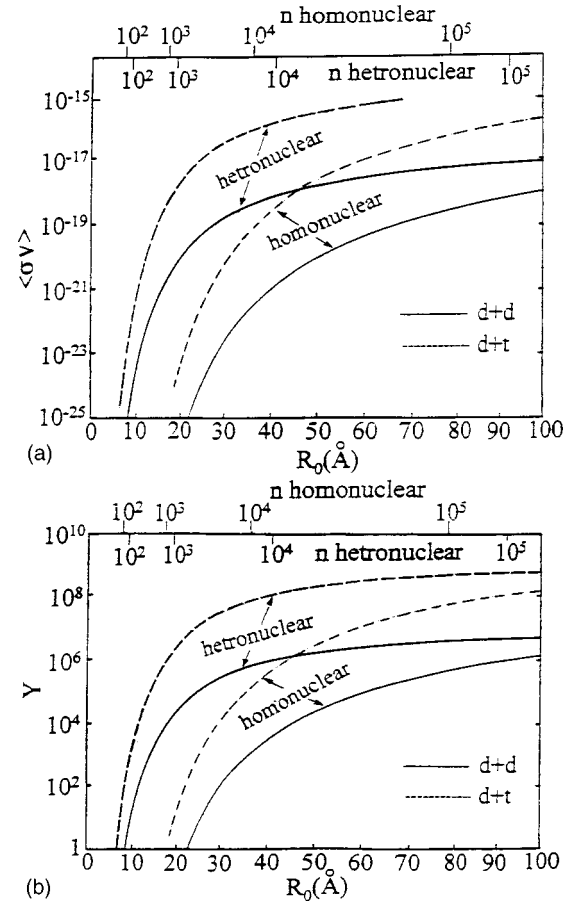


FIG. 13. The dependence of the nuclear fusion parameter  $\langle\sigma v\rangle$  and the neutron yield  $Y$  on the cluster radius  $R_0$ . The number of atoms  $n$  corresponding to  $R_0$  are shown on the upper scale for homonuclear and heteronuclear clusters. (a) The parameter  $\langle\sigma v\rangle$ . (b) The neutron yield  $Y$ .

heteronuclear clusters, it is determined for the laser power  $I = 2 \times 10^{18} \text{ W cm}^{-2}$  (Fig. 10). Both the  $\langle \sigma v \rangle$  [Fig. 13(a)] and the  $Y$  [Fig. 13(b)] dependences on  $R_0$  demonstrate significant differences between homonuclear and heteronuclear clusters, favouring NFDCE for heteronuclear clusters. As already noted, the fusion yield for the  $d+t$  reaction is higher than for the  $d+d$  reaction, both for homonuclear and heteronuclear clusters [Fig. 13(b)]. The largest yields are obtained from the NFDCE  $d+t$  reaction for heteronuclear  $(\text{D}_2\text{O}, \text{T}_2\text{O})_{n/2}$  clusters. It is also interesting to note that the yields for the  $d+t$  reaction from homonuclear clusters exceed those for the  $d+d$  reaction from heteronuclear clusters for  $R_0 > 50 \text{ \AA}$  [Fig. 13(b)].

The results presented in Fig. 13(b) can be compared with the NFDCE experimental data for  $dd$  fusion provided by homonuclear  $\text{D}_n$  clusters [12,13]. According to these experimental data, the neutron yield increases from  $Y \approx 10$  at  $\bar{R}_0 \approx 16 \text{ \AA}$  up to  $Y \approx 3 \times 10^3$  at  $\bar{R}_0 \sim 20\text{--}25 \text{ \AA}$ , where  $\bar{R}_0$  is the average cluster radius. According to our computation results [Fig. 13(b)] such an increase in the yield  $Y$  is provided for the cluster size interval  $R_0 = 27\text{--}40 \text{ \AA}$ . In a detailed comparison of our results with the experimental data [12,13], we have to account for the experimental cluster-size distribution, which is unknown. At present, we may conclude that our results are consistent with the gross features of the experimental data.

## VI. CONCLUDING REMARKS

The efficiency of nuclear fusion depends strongly on the energy spectrum of the colliding nuclei [14,37,38]. In the case of NFDCE, the energy spectrum of the  $\text{D}^+$  and  $\text{T}^+$  ions differs significantly from the thermal energy spectrum and is characterized by a maximal energy  $E_M$  presented by Eqs. (7) and (9) (Figs. 9 and 11) and an energy distribution as described by Eqs. (8) and (11). It follows that the results ob-

tained for the thermonuclear fusion cannot be unconditionally applied to our case. In order to deal with NFDCE, we calculated the dependence of the fusion parameter  $\langle \sigma v \rangle$  and the yield  $Y$  on the maximal energy  $E_M$  for the energy spectra provided by clusters (Fig. 12).

The maximization of the NFDCE yields can be accomplished by optimizing the  $\text{D}^+$  and  $\text{T}^+$  maximal energy at sufficiently high laser intensities, by the application of  $d+d$  or  $d+t$  NFDCE of heteronuclear clusters, and by the use of the  $d+t$  fusion reaction. According to our simulation results, the maximal energy  $E_M$  increases with laser intensity  $I$  up to intensities providing fusion saturation (Figs. 9 and 10). In order to maximize the fusion efficiency, one has to apply the saturation (or sometimes near-saturation) intensities. Using these intensities for the  $E_M$  dependence on cluster radius  $R_0$  and for the  $\langle \sigma v \rangle$  dependence on  $E_M$  (Fig. 12), we found the  $\langle \sigma v \rangle$  and the reaction yield  $Y$  dependence on cluster radius  $R_0$  (Fig. 13). Figure 13 demonstrates the important advantage of the heteronuclear clusters as against homonuclear clusters. For example, the  $d+d$  reaction yield of  $Y = 10^2$  per pulse is provided by homonuclear  $\text{D}_n$  clusters with  $R_0 = 30 \text{ \AA}$  and  $n = 5600$ , whereas the same yield can provide heteronuclear  $(\text{D}_2\text{O})_n$  clusters with a much smaller radius of  $R_0 = 12 \text{ \AA}$  and  $n = 250$ . Finally, we predict that a reaction yield of about two orders of magnitude larger than that of the  $d+d$  reaction is provided by the reaction  $d+t$  [Eq. (1b)]. This reaction can be realized by NFDCE of clusters consisting of both D and T atoms, such as  $(\text{DT})_{n/2}$  and  $(\text{D}_2\text{O}, \text{T}_2\text{O})_{n/2}$ .

## ACKNOWLEDGMENTS

This research was supported by the Binational German-Israeli James Frank program on Laser-Matter Interaction. We are grateful to Professor V. P. Krainov for stimulating correspondence and the prepublication information.

- 
- [1] J. Purnell, E. M. Snyder, S. Wei, and A. W. Castleman, Jr., *Chem. Phys. Lett.* **229**, 333 (1994).
  - [2] J. V. Ford, O. Zhong, L. Poth, and A. W. Castleman, Jr., *J. Chem. Phys.* **110**, 6257 (1999).
  - [3] J. Kou, N. Nakashima, S. Sakabe, S. Kawato, H. Ueyama, T. Urano, T. Kuge, Y. Izawa, and Y. Kato, *Chem. Phys. Lett.* **289**, 334 (1998).
  - [4] J. Kou *et al.*, *J. Chem. Phys.* **112**, 5012 (2000).
  - [5] T. Ditmire, T. Donnelly, A. M. Rubenchik, R. W. Falcone, and M. D. Perry, *Phys. Rev. A* **53**, 3379 (1996).
  - [6] T. Ditmire, J. W. G. Tisch, E. Springate, M. B. Mason, N. Hay, R. A. Smith, J. Marangos, and M. H. R. Hutchinson, *Nature (London)* **386**, 54 (1997).
  - [7] T. Ditmire, J. W. G. Tisch, E. Springate, M. B. Mason, N. Hay, J. P. Marangos, and M. H. R. Hutchinson, *Phys. Rev. Lett.* **78**, 2732 (1997).
  - [8] M. H. R. Hutchinson, T. Ditmire, E. Springate, J. W. G. Tisch, Y. L. Shao, M. B. Mason, N. Hay, and J. P. Marangos, *Philos. Trans. R. Soc. London, Ser. A* **356**, 297 (1998).
  - [9] T. Ditmire, E. Springate, J. W. G. Tisch, Y. L. Shao, M. B. Mason, N. Hay, J. P. Marangos, and M. H. R. Hutchinson, *Phys. Rev. A* **57**, 369 (1998).
  - [10] E. Springate, N. Hay, J. W. G. Tisch, M. B. Mason, T. Ditmire, M. H. R. Hutchinson, and J. P. Marangos, *Phys. Rev. A* **57**, 063201 (2000).
  - [11] M. Lezius, S. Dobosh, D. Normand, and M. Schmidt, *Phys. Rev. Lett.* **80**, 261 (1998).
  - [12] J. Zweiback, R. A. Smith, T. E. Cowan, G. Hays, K. B. Wharton, V. P. Yanovsky, and T. Ditmire, *Phys. Rev. Lett.* **84**, 2634 (2000).
  - [13] J. Zweiback, T. E. Cowan, R. A. Smith, J. H. Hurlay, R. Howell, C. A. Steinke, G. Hays, K. B. Wharton, J. K. Krane, and T. Ditmire, *Phys. Rev. Lett.* **85**, 3640 (2000).
  - [14] S. Glasstone and R. H. Lovberg, *Controlled Thermonuclear Reactions* (Van Nostrand, Princeton, 1960).
  - [15] I. Last and J. Jortner, *Phys. Rev. Lett.* **87**, 033401 (2001).
  - [16] I. Last and J. Jortner, *Phys. Rev. A* **62**, 013201 (2000).
  - [17] K. Boyer, T. S. Luk, J. C. Solem, and C. K. Rhodes, *Phys. Rev. A* **39**, 1186 (1989).

- [18] J. Jortner and R. D. Levine, *Isr. J. Chem.* **30**, 207 (1990).
- [19] I. Last, I. Schek, and J. Jortner, *J. Chem. Phys.* **107**, 6685 (1997).
- [20] T. Ditmire, *Phys. Rev. A* **57**, R4094 (1998).
- [21] I. Last and J. Jortner, *Phys. Rev. A* **60**, 2215 (1999).
- [22] K. Ishikawa and Th. Blenski, *Phys. Rev. A* **62**, 063204 (2000).
- [23] P. B. Corcum, *Phys. Rev. Lett.* **71**, 1994 (1993).
- [24] W. Lotz, *Z. Phys.* **216**, 241 (1968).
- [25] V. P. Krainov and M. B. Smirnov, *Usp. Fiz. Nauk* **170**, 969 (2000).
- [26] A. Talebpour, K. Vijayalakshmi, A. S. D. Bandrauk, T. T. Nguyen-Dang, and S. L. Chin, *Phys. Rev. A* **62**, 042708 (2000).
- [27] C. Rose-Petruck, K. J. Schafer, K. R. Wilson, and C. P. J. Barty, *Phys. Rev. A* **55**, 1182 (1997).
- [28] I. Last and T. F. George, *J. Chem. Phys.* **93**, 8925 (1990).
- [29] A. Goldberg, I. Last, and T. F. George, *J. Chem. Phys.* **100**, 8277 (1994).
- [30] *Kirk-Othmer Encyclopedia of Chemical Technology*, 3d ed. (Wiley, New York, 1979), Vol. 7, p. 541.
- [31] J. Jortner, *Z. Phys. D: At., Mol. Clusters* **24**, 247 (1992).
- [32] J. Jortner, *J. Chim. Phys. Phys.-Chim. Biol.* **92**, 205 (1995).
- [33] E. Teller, *Fusion* (Academic, New York, 1981).
- [34] H. S. Massey and H. B. Gilbody, *Electronic and Ionic Impact Phenomena* (Oxford University, New York, 1974), Vol. 4.
- [35] P. M. Echenique, J. R. Manson, and R. H. Ritchie, *Phys. Rev. Lett.* **64**, 1413 (1990).
- [36] R. J. Buehler, G. Friedlander, and L. Friedman, *Phys. Rev. Lett.* **63**, 1292 (1989).
- [37] L. A. Artsimovich, *Controlled Thermonuclear Reactions* (Gordon and Breach, New York, 1964).
- [38] D. J. Rose and M. Clark, Jr., *Plasmas and Controlled Fusion* (MIT Cambridge, MA, 1961).